Research Square

Preprints are preliminary reports that have not undergone peer review.
They should not be considered conclusive, used to inform clinical practice,
or referenced by the media as validated information.

Biomechanical comparison of fixation strategies for rotator cuff repair in simulated osteoporotic bone using pullout testing and finite element analysis

Qi Zhang
The Affiliated Hospital of Southwest Medical University
Wuxiang Wang
Zhaotong First People's Hospital
Yu Zheng
Gaoxian Hospital of Traditional Chinese Medicine
Shunlin Zhang
Tianfu Hospital Affiliated to Southwest Medical University
Jinhui Liu
The Affiliated Hospital of Southwest Medical University
Hongbin Yang
yanghongbin1234@163.com

The Affiliated Hospital of Southwest Medical University

Research Article

Keywords: Rotator cuff repair, Osteoporosis, Suture anchor, Cement augmentation, Transosseous fixation, Biomechanics, Finite element analysis

Posted Date: November 5th, 2026

DOI: https://doi.org/10.21203/rs.3.rs-11235549/v1

License: This work is licensed under a Creative Commons Attribution 4.0 International License.
Read Full License

Additional Declarations: No competing interests reported.

Biomechanical comparison of fixation strategies for rotator cuff repair in simulated osteoporotic bone using pullout testing and finite element analysis

Article type: Research article

Qi Zhang[1]†, Wuxiang Wang[2]†, Yu Zheng[3], Shunlin Zhang[4], Jinhui Liu[5]*, Hongbin Yang[1]*

1 Department of Bone and Joint Surgery, The Affiliated Hospital of Southwest Medical University, 25 Taiping Street, Jiangyang District, Luzhou, Sichuan, China.

2 Department of Orthopaedics, Zhaotong First People's Hospital, 35 Yiwei Road, Zhaoyang District, Zhaotong, Yunnan, China.

3 Department of Orthopaedics, Gaoxian Hospital of Traditional Chinese Medicine, 137 Wenmiao Street, Qingfu Town, Gao County, Yibin, Sichuan, China.

4 Department of Orthopaedics, Tianfu Hospital Affiliated to Southwest Medical University, 168 Huantianfu New Area Expressway, Shigao Subdistrict, Meishan Tianfu New Area, Meishan, Sichuan, China.

5 Sichuan Provincial Engineering Laboratory for Research, Development and Application of Orthopaedic Implant Devices, 63 Buchang Road, Lu County, Luzhou, Sichuan, China.

† Qi Zhang and Wuxiang Wang contributed equally to this work and share first authorship.

* Correspondence: Hongbin Yang, yanghongbin1234@163.com; Jinhui Liu, liujinhuiswmu@163.com.

Abstract

Background: Poor bone quality can compromise suture anchor fixation during rotator cuff repair. This study compared five fixation strategies in a standardized model of osteoporotic bone and explored their mechanical behavior using finite element analysis.

Methods: Six groups of eight polyurethane foam constructs were tested: five osteoporotic configurations comprising non-reinforced single anchors, cement-augmented anchors, buddy

anchors, conventional transosseous sutures, and transosseous suture tape, plus a higher-density non-reinforced anchor reference group. Anchor constructs were loaded through steel wire, whereas transosseous constructs used suture or tape. Axial loading was applied at 1 mm/s. Failure loads were summarized as means and standard deviations and compared using one-way analysis of variance with post hoc comparisons. Five CT-based finite element models were used to explore displacement and stress distributions.

Results: The mean ultimate failure load was 122.17 ± 10.08 N in the osteoporotic non-reinforced anchor group and 279.97 ± 18.38 N in the higher-density reference group ($P < 0.001$). Under osteoporotic conditions, cement augmentation had the highest mean failure load (338.55 ± 28.52 N), followed by transosseous suture tape fixation (201.05 ± 22.55 N), buddy anchor fixation (192.96 ± 12.78 N), and conventional transosseous suture fixation (116.00 ± 9.79 N). No statistically significant differences were detected between conventional transosseous and non-reinforced anchor fixation ($P = 0.9882$), or between buddy anchor and transosseous suture tape fixation ($P = 0.9612$). The simulations suggested different patterns of load transfer at the anchor interface and lateral bone tunnel outlet.

Conclusions: Cement augmentation produced the highest initial fixation strength under the tested conditions. Buddy anchor and transosseous suture tape fixation provided intermediate failure loads. These findings concern initial fixation in a simplified model and do not establish clinical superiority or resistance to repeated loading.

Keywords: Rotator cuff repair; Osteoporosis; Suture anchor; Cement augmentation; Transosseous fixation; Biomechanics; Finite element analysis

Background

Degenerative rotator cuff tears are an important cause of shoulder dysfunction, and treatment decisions depend on tear characteristics and patient factors [1]. Suture anchor fixation is widely used in repair, but failure can occur at different interfaces within the repair construct [2]. The capacity of the bone–anchor interface to withstand loading is particularly relevant

when bone quality is poor. Previous work has related anchor pullout strength to local bone mineral density [3], and early anchor pullout has been reported after arthroscopic repair [4]. Several strategies have been proposed to improve fixation when anchor purchase is inadequate. Polymethylmethacrylate (PMMA) cement augmentation can improve fixation in cadaveric humeri [5]. A polyurethane foam study also examined augmentation in osteopenic and severely osteoporotic models [6]. Adjacent, or buddy, anchors provide another option for managing a loose anchor [7], while the broader management of poor-quality bone and tissue may require changes to the repair construct [8].

Transosseous fixation transfers load through bone tunnels rather than relying on an anchor. Its performance depends on the bone–suture interface as well as tunnel geometry and suture properties. Braided tape has shown greater bone pull-through strength than conventional wire suture in a cadaveric greater tuberosity study [9]. However, these findings do not establish how tape-based fixation compares with cement augmentation or buddy anchors under the same low-density bone conditions.

Existing augmentation studies address important aspects of anchor fixation, but differences in bone models, implants and loading protocols complicate comparisons between techniques [5,6,10]. The present study therefore compared non-reinforced anchor fixation, cement-augmented anchor fixation, buddy anchor fixation, conventional transosseous suture fixation and transosseous suture tape fixation within a standardized osteoporotic foam model. Axial failure testing was combined with an exploratory finite element analysis to examine initial fixation strength and potential differences in load transfer.

Methods

Study design

This laboratory study combined destructive axial testing of synthetic bone constructs with finite element analysis of five fixation configurations. The primary experimental outcome

was ultimate failure load. A higher-density non-reinforced single anchor construct was included as a reference for the combined effect of cancellous foam density and cortical layer thickness. Eight specimens were prepared for each of six groups, giving 48 constructs. The sample size was selected on practical grounds, including material cost, rather than a reported a priori power calculation.

Synthetic bone model preparation

Open-cell polyurethane foam of 7.5 lb/ft³ (approximately 120 kg/m³) and 15 lb/ft³ (approximately 240 kg/m³) represented osteoporotic and higher-density cancellous bone, respectively. The cancellous blocks measured 50 × 60 × 40 mm. Closed-cell foam of 30 lb/ft³ (approximately 480 kg/m³) represented the cortical layer. Plates measuring 50 × 60 mm were 2 mm thick for osteoporotic constructs and 3 mm thick for the higher-density reference constructs. Corresponding layers were bonded with epoxy resin and allowed to bond firmly before testing (Fig. 1). Polyurethane models have previously been used in studies of augmented suture anchor fixation [6,10].

The two model conditions differed in both cancellous density and cortical layer thickness. Accordingly, the between-model comparison assessed the combined effect of these features rather than the independent effect of bone mineral density.

Fixation configurations

The osteoporotic non-reinforced single anchor group (OS-NRSA) and higher-density reference group (ND-NRSA) used 5.0-mm fully threaded metallic anchors. A 4.0-mm Kirschner wire was used to prepare a pilot hole perpendicular to the cortical surface to a depth of 20 mm before anchor insertion. In all anchor groups, the original suture was replaced by 0.6-mm-diameter steel wire to reduce the likelihood of suture rupture during testing. The transosseous groups retained suture or tape as their loading connectors.

In the osteoporotic bone cement-augmented anchor group (OS-BCRA), the anchor was first inserted into the pilot hole and then unscrewed to prepare the insertion channel. Cement was mixed according to the manufacturer's instructions. Approximately 1 mL was injected through a 5-mL syringe during the stringy phase, and the anchor was immediately reinserted. The cement was allowed to cure for 24 h before testing. The selected volume was informed by preliminary work in the same cadaveric humerus subsequently used for CT-based finite element reconstruction, and radiographs were obtained after setting to assess cement distribution in the foam constructs (Fig. 2). The channel was not subjected to destructive pullout before augmentation.

In the osteoporotic buddy anchor group (OS-BDA), the first anchor was inserted as described for OS-NRSA. While tension was maintained on the primary anchor, a second pilot hole was drilled with a 4.0-mm Kirschner wire immediately adjacent to its thread surface. A second anchor was inserted to interlock the threads of the two anchors. Mechanical loading was applied to the primary anchor only.

For the two transosseous groups, an additional 2-mm-thick layer of 30 lb/ft³ closed-cell foam was bonded to the lateral surface with epoxy resin. A 4.0-mm Kirschner wire created two perpendicular communicating tunnels. The vertical tunnel entered the top surface 15 mm from the lateral side and extended 15 mm in depth. The horizontal tunnel entered the lateral surface 15 mm below the top and extended 15 mm to meet the vertical tunnel. The osteoporotic conventional transosseous suture group (OS-STS) used No. 2 FiberWire passed through the tunnels and tied. The osteoporotic transosseous suture tape group (OS-STTS) used the same tunnel configuration with 2-mm-wide tape (Smith & Nephew).

Axial loading to failure

Each construct was secured in an Instron E10000 testing machine using a custom clamp mounted on an XY positioning platform. The steel wire, suture or tape was formed into a loop and connected to a traction hook. Approximately 1 N of preload was applied, followed

by axial tensile loading at 1 mm/s. Failure was defined as a sudden decrease in the load–displacement curve or displacement reaching 10 mm. The highest force recorded up to this endpoint was defined as the ultimate failure load.

The term ultimate failure load is used across all groups because transosseous constructs do not contain an anchor and their failure need not involve anchor pullout. The protocol assessed initial strength under monotonic loading; cyclic loading was not performed.

Finite element model construction

The finite element geometry was reconstructed from a right cadaveric humerus from a 75-year-old male donor, supplied by the Department of Anatomy, Southwest Medical University. The specimen had no reported deformity or tumor and a reported bone mineral density of 0.495 g/cm². This was the same humerus used in the preliminary cement-augmentation work illustrated in Fig. 2A. CT images were acquired using a Philips 128-row scanner before and after cement-augmented anchor insertion. The recorded slice interval and thickness were 1.0 and 0.55 mm, respectively. DICOM images were segmented by thresholding and filling in Mimics 25.0 to reconstruct the humerus and cement. STL models were repaired, smoothed and fitted in Geomagic 2021 (Fig. 3).

Anchor geometry was acquired using a KSCAN-MAGIC three-dimensional scanner. The humerus, anchor and cement geometries were assembled in 3-Matic. Sutures were modeled with a diameter of 0.6 mm, and tape with a width of 2 mm and thickness of 0.6 mm. The five fixation configurations are shown in Fig. 4. Anchors were positioned approximately 10 mm posterior to the bicipital groove, at the junction of the greater tuberosity and articular cartilage, with their axes parallel to the humeral axis. The buddy anchor was placed immediately posterior to the primary anchor with interlocking threads. Transosseous tunnel entry sites were located at the greater tuberosity–cartilage junction and on the lateral surface 15 mm below the lateral edge of the greater tuberosity.

Material properties and boundary conditions

Humeral material properties were assigned from CT grayscale values in Mimics (Fig. 5). The recorded mapping was $\rho = -0.009 + 0.0007 \times HU$, where ρ is density in g/cm³ and HU is the CT value in Hounsfield units. Young's modulus E, in MPa, was calculated as 14,664 multiplied by ρ raised to the power 1.49. The non-bone material parameters are listed in Table 1. Previous finite element studies provide broader methodological context [11–13]. The distal cut surface of the humerus was fully constrained, and loading was applied parallel to the humeral axis (Fig. 6). Sliding was permitted at the specified fixation–bone interfaces. The recorded friction coefficients were 0.30 for cement–bone contact, 0.40 for anchor–bone contact, and 0.46 for suture/tape–bone contact. The remaining interfaces were described as tied. Anchor orientation and loading direction may influence local stress distributions [14].

Table 1 Material parameters reported for the finite element models

Material	Young's modulus (MPa)	Poisson's ratio
Titanium alloy anchor	11000	0.28
PMMA cement	3000	0.40
Suture / suture tape	10729	0.40

Values are retained from the original manuscript. See AQ08 for verification of the anchor modulus and parameter sources. Bone properties require the CT-to-material mapping described in Methods.

Numerical verification and outcome measures

The humerus, anchors, cement, sutures and tape were meshed in 3-Matic using four-node tetrahedral solid elements (C3D4). Model-specific node and element counts are reported in Table 2. The finite element outcomes were maximum displacement, stress distribution and maximum von Mises equivalent stress. These outputs were used to explore possible load-

transfer mechanisms; stress localization alone was not interpreted as experimental evidence of material failure.

Table 2 Node and element counts in the finite element models

Model	Nodes	Elements
OS-NRSA	38952	175434
OS-BCRA	42859	186815
OS-BDA	67438	293661
OS-STS	56011	233342
OS-STTS	124610	498371

All components were meshed using C3D4 elements. Mesh counts do not establish mesh convergence (AQ09).

Statistical analysis

Analyses were performed in GraphPad Prism 10.1.2. Continuous data were assessed using the Shapiro–Wilk test and summarized as mean ± standard deviation (SD). The six experimental groups were compared using one-way analysis of variance followed by pairwise post hoc comparisons. The significance threshold was $P < 0.05$. Individual finite element model outputs were reported descriptively and were not treated as replicated experimental measurements.

Use of artificial intelligence in manuscript preparation

An OpenAI large language model was used to assist with English-language revision, manuscript organization and identification of reporting inconsistencies. It was not used to generate experimental observations or finite element simulation outputs.

Results

Failure load in the two synthetic bone conditions

Ultimate failure loads are summarized in Table 3 and Fig. 7. The mean failure load was 279.97 ± 18.38 N in ND-NRSA and 122.17 ± 10.08 N in OS-NRSA ($P < 0.001$). This corresponds to an approximately 56.4% lower mean failure load in the construct combining lower-density cancellous foam and a thinner cortical layer.

Table 3 Ultimate failure loads of the fixation constructs

Group	Ultimate failure load (N)
ND-NRSA	279.97 ± 18.38
OS-NRSA	122.17 ± 10.08
OS-BCRA	338.55 ± 28.52
OS-BDA	192.96 ± 12.78
OS-STS	116.00 ± 9.79
OS-STTS	201.05 ± 22.55

Data are mean ± SD; n = 8 per group. Values follow the results table because the bar chart does not label exact means or SDs. The source selection follows the author-approved hierarchy (AQ02). Group abbreviations are defined in the list of abbreviations.

Comparison of fixation strategies under osteoporotic conditions

The overall comparison across the six experimental groups was reported as statistically significant ($P < 0.0001$). OS-BCRA had the highest mean ultimate failure load, 338.55 ± 28.52 N, representing an approximately 177.1% increase relative to OS-NRSA. Its mean failure load also exceeded that of ND-NRSA.

The mean failure loads were 192.96 ± 12.78 N for OS-BDA and 201.05 ± 22.55 N for OS-STTS. OS-BDA therefore had a mean failure load approximately 57.9% higher than OS-

NRSA. The mean load in OS-STS was 116.00 ± 9.79 N. Post hoc comparisons did not detect differences between OS-NRSA and OS-STS (P = 0.9882), or between OS-BDA and OS-STTS (P = 0.9612). All remaining pairwise comparisons were reported as significant (P < 0.0001), subject to verification of the test and its output (AQ10). The non-significant comparisons do not establish equivalence.

Observed failure modes

Single-anchor pullout was described in ND-NRSA and OS-NRSA. In OS-BCRA, the anchor and surrounding cement were extracted together. In OS-BDA, the two interlocked anchors were pulled out together. Both transosseous groups showed cutting of the simulated cortical layer at the lateral outlet of the horizontal tunnel. Representative post-test appearances are shown in Fig. 8.

Exploratory finite element findings

Using the group assignments in the current Fig. 9 legend, the displayed displacement values were 0.4450 mm for OS-NRSA (panel A), 0.02454 mm for OS-BDA (panel C), 0.01520 mm for OS-STS (panel D), and 0.1229 mm for OS-STTS (panel E). Panel B displays S, Mises rather than displacement, so no displacement value is reported here for OS-BCRA. The stress values displayed in Fig. 10 were 103.3 MPa for OS-NRSA, 51.80 MPa for OS-BCRA, 246.4 MPa for OS-BDA, 246.4 MPa for OS-STS, and 265.2 MPa for OS-STTS. These are transcriptions of the numerical extrema displayed in the figures under their current group labels; the labeling and output-region limitations are specified in AQ13.

The simulations were described as showing stress around the anchor interface in OS-NRSA, transfer through the cement–bone interface in OS-BCRA, and stress around both anchors in OS-BDA. In the transosseous constructs, stress was concentrated near the lateral cortical tunnel outlet. These observations suggest possible differences in load transfer, but their

quantitative interpretation requires confirmation of the loading conditions, output regions and figure consistency.

Discussion

This study compared the initial fixation performance of five constructs within a standardized low-density synthetic bone model. Cement augmentation produced the highest mean failure load, while buddy anchor fixation and transosseous suture tape fixation produced intermediate values. Conventional transosseous suture fixation did not show a statistically detectable improvement over non-reinforced anchor fixation. The main contribution is the comparison of these options under a common experimental setup, rather than a demonstration that cement augmentation can improve fixation for the first time.

The lower failure load in the osteoporotic construct is consistent with previous evidence that bone quality affects anchor fixation [3]. However, the present comparison changed both cancellous foam density and cortical layer thickness. The approximately 56.4% reduction therefore cannot be attributed to cancellous density alone or directly translated into the effect of osteoporosis in patients. The model provides controlled comparisons of constructs but does not reproduce the full spectrum of bone architecture or biological disease.

Cement augmentation has improved anchor fixation in previous cadaveric and foam studies [5,6]. The higher failure load observed here is consistent with that evidence. Load transfer through a cement mantle is a plausible explanation, and cement–bone interface behavior has been examined in micromechanical modeling [12]. Nevertheless, the current simulation requires verification before differences in peak stress can be used as strong mechanistic evidence. An ultimate failure load greater than that of the higher-density reference group does not establish superior repair healing, clinical safety or durability.

Buddy anchor fixation and transosseous suture tape fixation showed no statistically significant difference in failure load. Their load-transfer mechanisms differ: interlocked anchors may increase mechanical support around the fixation site, whereas wider tape may

distribute contact forces over a larger bone surface [7–9]. The observed joint pullout of the two anchors is compatible with mechanical interaction, but does not quantify the separate contributions of interference fit, cortical support and load sharing. Only the primary anchor was loaded in this experiment; the study therefore did not test any additional benefit from using sutures attached to both anchors. The absence of a significant difference does not establish clinical interchangeability.

Conventional transosseous fixation did not improve the measured endpoint relative to non-reinforced anchor fixation. Transosseous constructs avoid dependence on anchor purchase but remain dependent on tunnel geometry and cortical support. Cutting at the lateral cortical outlet was observed in both transosseous groups, consistent with the reported location of stress concentration. This agreement is qualitative and does not validate the predicted stress magnitude or establish a material failure threshold. The higher failure load with tape supports a benefit under the tested conditions, but does not demonstrate elimination of cortical cut-through.

Finite element analysis can complement mechanical testing by illustrating internal stress patterns that are difficult to measure directly. Its value depends on material assignments, contact conditions, mesh convergence and validation. In the present study, the finite element geometry came from one human humerus, whereas the mechanical tests used synthetic blocks. The simulations should therefore be regarded as exploratory mechanical analyses unless their relationship to the experimental constructs is established quantitatively. Peak stress alone, without an appropriate failure criterion, cannot establish failure load or failure mechanism.

The findings are relevant to the mechanical selection of fixation strategies when bone purchase is poor, but they do not support a universal clinical recommendation. Cement use also raises questions concerning leakage, thermal effects and later revision [8]. Decisions in surgery must account for the condition of the tendon, the repair configuration and the

properties of the available implants, none of which were fully represented by the isolated fixation tests.

Several limitations restrict interpretation. First, synthetic foam does not reproduce trabecular architecture, local variation, remodeling or tendon–bone healing. Second, the sample size was selected for practical reasons, and eight specimens per group provide limited information on variability. Third, monotonic axial loading does not reproduce repeated or multidirectional loading after repair. Fourth, anchor constructs were loaded through steel wire, whereas transosseous constructs were loaded through suture or tape; connector properties can affect construct displacement and failure behavior. The protocol primarily assessed initial bone-side fixation rather than a complete tendon repair. Fifth, the results depend on the tested implant geometry, cement volume, cortical layers and tunnel configuration. Sixth, the finite element analysis used a single human humerus rather than the foam geometry used for mechanical testing. Its load definition, material inputs, output regions, numerical verification and validation require confirmation. Maximum displacement may include connector deformation and should not automatically be interpreted as displacement at the fixation–bone interface. Finally, no clinical outcomes were assessed. Future work should examine cyclic loading and failure mechanisms in cadaveric constructs before assessing clinical effectiveness.

Conclusions

In the tested synthetic osteoporotic bone constructs, PMMA cement augmentation produced the highest ultimate failure load. Buddy anchor fixation and transosseous suture tape fixation yielded intermediate values, while conventional transosseous suture fixation did not show an improvement over non-reinforced anchor fixation. These results describe initial mechanical fixation under one loading protocol. Further validation is required before inferring resistance to repeated loading or clinical benefit.

List of abbreviations

CT, computed tomography; ND-NRSA, higher-density non-reinforced single anchor group; OS-NRSA, osteoporotic non-reinforced single anchor group; OS-BCRA, osteoporotic bone cement-augmented anchor group; OS-BDA, osteoporotic buddy anchor group; OS-STS, osteoporotic conventional transosseous suture group; OS-STTS, osteoporotic transosseous suture tape group; PMMA, polymethylmethacrylate; SD, standard deviation.

Declarations

Ethics approval and consent to participate

The study was approved by the Clinical Trial Ethics Committee of the Affiliated Hospital of Southwest Medical University (reference no. KY2026588; 24 September 2026). The approval included a waiver of the requirement for a signed informed consent form. The cadaveric humerus was supplied by the Department of Anatomy, Southwest Medical University.

Consent for publication

Availability of data and materials

Competing interests

The authors declare that they have no competing interests.

Funding

This work was supported by the provincial/ministerial-level project “Applied Anatomical Research on the Selection of Elbow Arthroscopy Portals in the Chinese Population” (project no. 13012).

Authors' contributions

Qi Zhang conceived and designed the study, performed the biomechanical experiments, and collected the data. Wuxiang Wang performed the finite element modeling and analysis. Yu Zheng organized the data and performed the statistical analyses. Shunlin Zhang drafted the manuscript. Jinhui Liu critically reviewed and revised the manuscript. Hongbin Yang supervised the study and provided resources. Qi Zhang and Wuxiang Wang contributed equally to this work and share first authorship.

Acknowledgements

The authors thank the Department of Anatomy, Southwest Medical University, for providing the cadaveric humeral specimen used in this study.

References

1. Keener JD, Patterson BM, Orvets N, Chamberlain AM. Degenerative rotator cuff tears: refining surgical indications based on natural history data. J Am Acad Orthop Surg. 2019;27(5):156–165.

2. Cummins CA, Murrell GAC. Mode of failure for rotator cuff repair with suture anchors identified at revision surgery. J Shoulder Elbow Surg. 2003;12(2):128–133.

3. Tingart MJ, Apreleva M, Lehtinen J, Zurakowski D, Warner JJP. Pullout strength of suture anchors used in rotator cuff repair. J Bone Joint Surg Am. 2003;85(11):2190–2194.

4. Benson EC, MacDermid JC, Drosdowech DS, Athwal GS. The incidence of early metallic suture anchor pullout after arthroscopic rotator cuff repair. Arthroscopy. 2010;26(3):310–315.

5. Giori NJ, Sohn DH, Mirza FM, Lindsey DP, Lee AT. Bone cement improves suture anchor fixation. Clin Orthop Relat Res. 2006;451:236–241.

doi:10.1097/01.blo.0000223984.67325.af.

6. Er MS, Altinel L, Eroglu M, Verim O, Demir T, Atmaca H. Suture anchor fixation strength with or without augmentation in osteopenic and severely osteoporotic bones in rotator cuff repair: a biomechanical study on polyurethane foam model. J Orthop Surg Res. 2014;9:48. doi:10.1186/1749-799X-9-48.

7. Brady PC, Arrigoni P, Burkhart SS. What do you do when you have a loose screw? Arthroscopy. 2006;22(9):925–930.

8. Denard PJ, Burkhart SS. Techniques for managing poor quality tissue and bone during arthroscopic rotator cuff repair. Arthroscopy. 2011;27(10):1409–1421.

9. Leger St-Jean B, Menard J, Hinse S, Petit Y, Rouleau DM, Beauchamp M. Braided tape suture provides superior bone pull-through strength than wire suture in greater tuberosity of the humerus. J Orthop. 2015;12 Suppl 1:S14–S17. doi:10.1016/j.jor.2015.01.025.

10. Diaz MA, Branch EA, Paredes LA, Oakley E, Baker CE. Calcium phosphate bone void filler increases threaded suture anchor pullout strength: a biomechanical study. Arthroscopy. 2020;36(4):1000–1008.

11. Sano H, Tokunaga M, Noguchi M, Inawashiro T, Irie T, Abe H, et al. Comparison of fixation properties between coil-type and screw-type anchors for rotator cuff repair: a virtual pullout testing using 3-dimensional finite element method. J Orthop Sci. 2016;21(4):452–457. doi:10.1016/j.jos.2016.04.011.

12. Janssen D, Mann KA, Verdonschot N. Micro-mechanical modeling of the cement-bone interface: the effect of friction, morphology and material properties on the micromechanical response. J Biomech. 2008;41(15):3158–3163. doi:10.1016/j.jbiomech.2008.08.020.

13. Mantovani M, Pellegrini A, Garofalo P, Baudi P. A 3D finite element model for geometrical and mechanical comparison of different supraspinatus repair techniques. J Shoulder Elbow Surg. 2016;25(4):557–563. doi:10.1016/j.jse.2015.09.002.

14. Sano H, Takahashi A, Chiba D, Hatta T, Yamamoto N, Itoi E. Stress distribution inside bone after suture anchor insertion: simulation using a three-dimensional finite element

method. Knee Surg Sports Traumatol Arthrosc. 2013;21(8):1777–1782. doi:10.1007/s00167-012-2060-0.

Figure legends

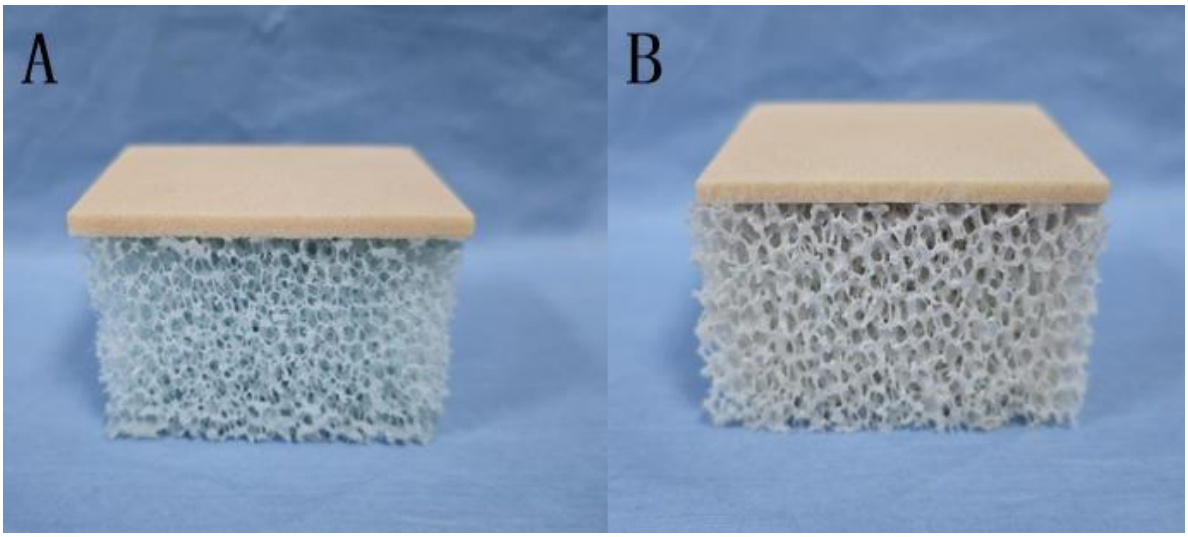


Fig. 1 Synthetic bone constructs. A, Osteoporotic construct with 7.5 lb/ft³ cancellous foam and a 2-mm cortical layer. B, Higher-density reference construct with 15 lb/ft³ cancellous foam and a 3-mm cortical layer.

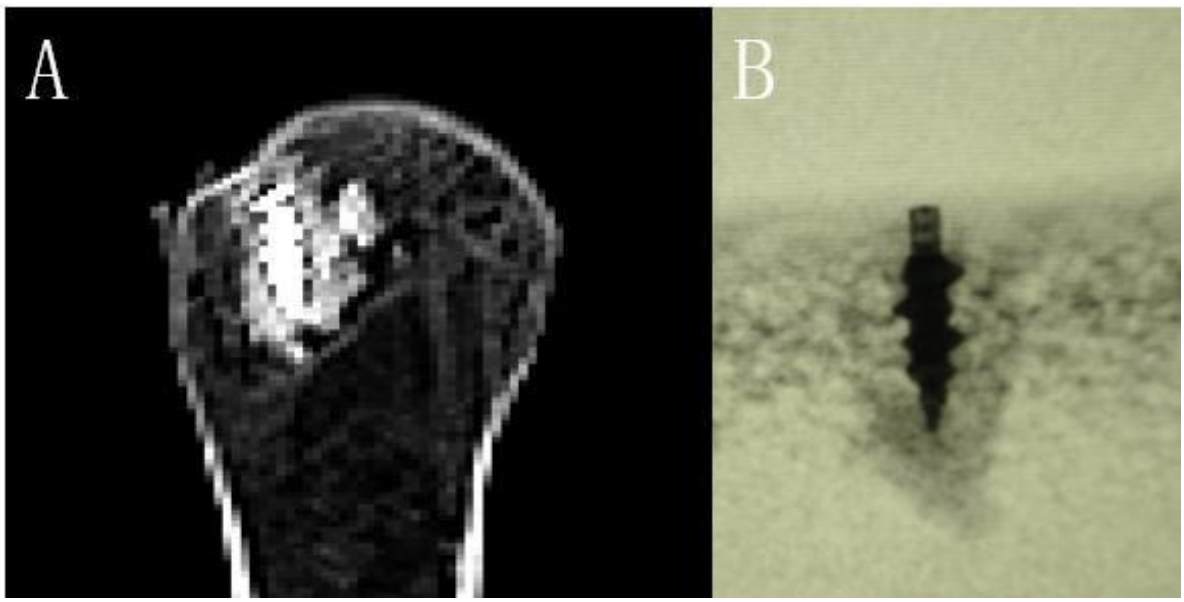


Fig. 2 Cement-augmented anchor fixation. A, Image of the cadaveric humerus used in preliminary cement-augmentation work and subsequent finite element reconstruction, informing the approximately 1-mL cement volume. B, Cement-augmented anchor in a synthetic bone construct.



Fig. 3 Reconstructed humeral geometry. Surface reconstruction of the humeral model using Geomagic.

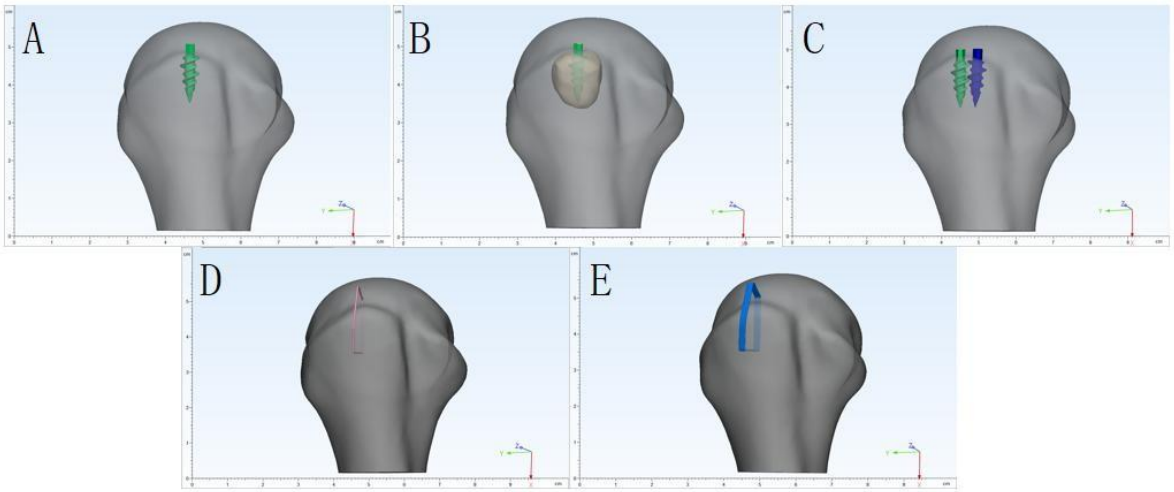


Fig. 4 Finite element fixation configurations. A, OS-NRSA. B, OS-BCRA. C, OS-BDA. D, OS-STS. E, OS-STTS. Abbreviations are defined in the list of abbreviations.

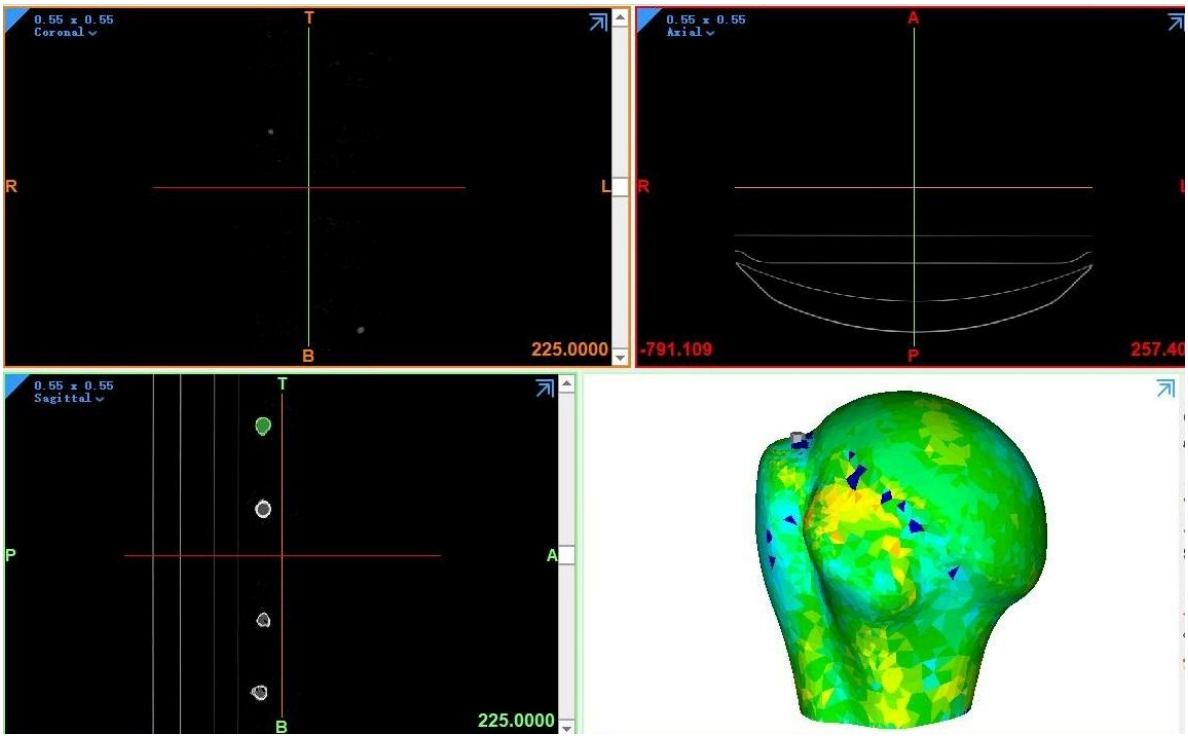


Fig. 5 CT-based assignment of humeral material properties. Illustration of the grayscale-based material-assignment workflow in Mimics.

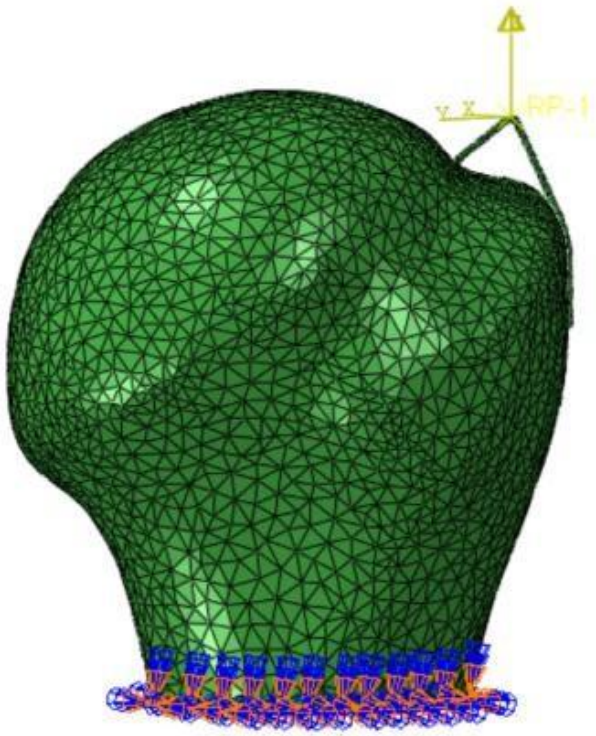


Fig. 6 Finite element constraints and loading direction. The distal cut surface was constrained in all directions. The arrow indicates loading parallel to the humeral axis.

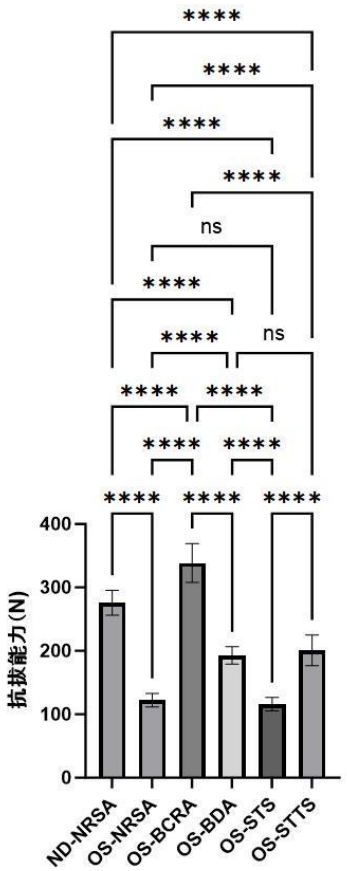


Fig. 7 Ultimate failure loads of the six fixation groups. Group abbreviations are defined in the list of abbreviations. Mean ± SD values are provided in Table 3.

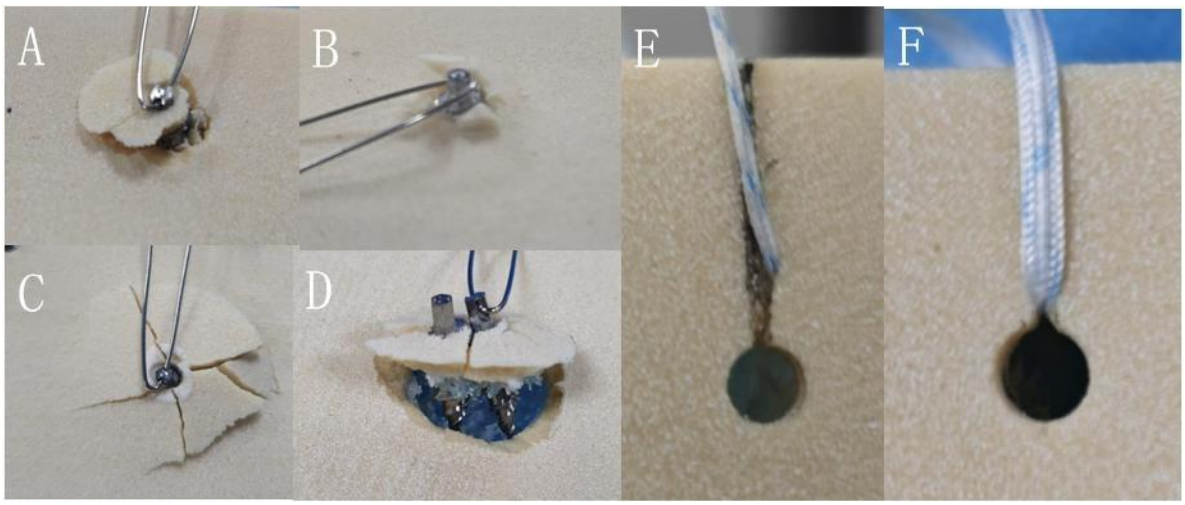


Fig. 8 Representative failure appearances. A, ND-NRSA single-anchor pullout. B, OS-NRSA single-anchor pullout. C, Anchor and cement extracted together in OS-BCRA. D, Joint pullout of the two anchors in OS-BDA. E and F, Lateral cortical cutting in OS-STS and OS-STTS, respectively.

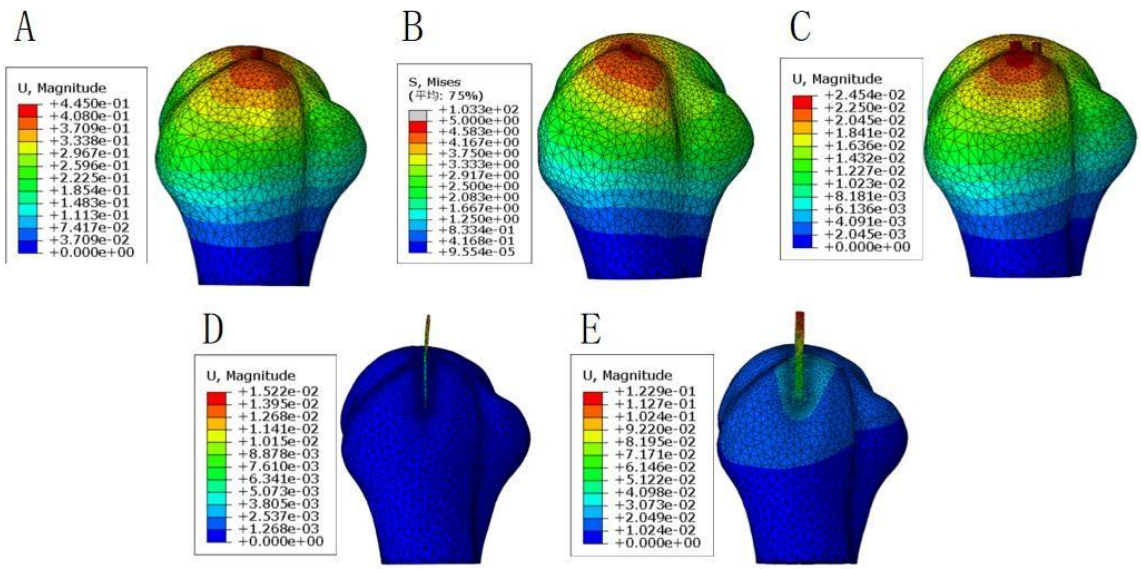


Fig. 9 Displacement distributions in the five finite element models. Intended group order: A, OS-NRSA; B, OS-BCRA; C, OS-BDA; D, OS-STS; E, OS-STTS. Numerical displacement readings are transcribed in Results using these group labels. Panel B currently displays stress and does not provide a displacement measurement (AQ13). Displacement units require confirmation as millimeters.

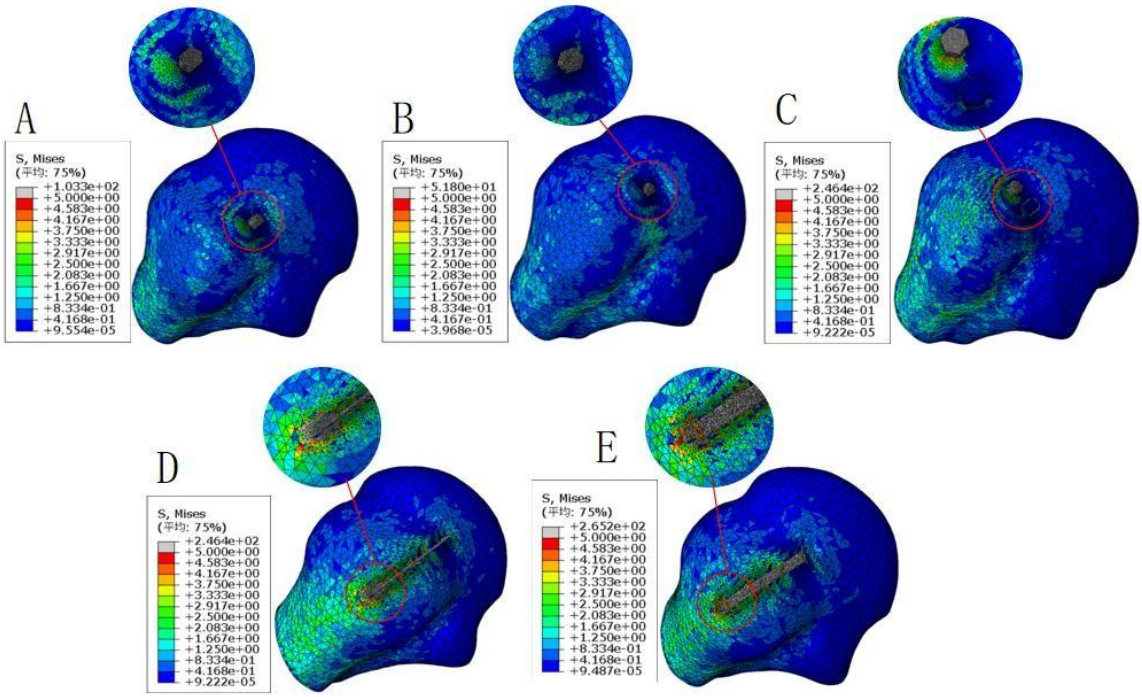


Fig. 10 Equivalent stress distributions in the five finite element models. Intended group order: A, OS-NRSA; B, OS-BCRA; C, OS-BDA; D, OS-STS; E, OS-STTS. The displayed maxima are 103.3, 51.80, 246.4, 246.4 and 265.2, respectively; units are treated as megapascals in the

417 manuscript, subject to confirmation of the model unit system. The C/D maxima and output
418 regions require verification (AQ13).